4-2017

Explorations of Quantum Entanglement

John Stanton
DePauw University

Explorations of Quantum Entanglement

John Stanton

Honor Scholar Program Senior Project

2017

Sponsor: Dr. John Caraher

Committee: Dr. Jeffrey Dunn, Dr. Andrea Clark, Dr. Douglas Harms

I. ABSTRACT

This thesis develops an undergraduate level understanding of quantum entanglement by expressing its properties in three unique mediums: mathematical formalism, application in technology and experiment. The mathematical formalism of entanglement is developed by working through theoretical experiments that utilize the entangled polarization states of photons. Notation used to describe entangled photon states is then used to illustrate how other types of entangled quantum states can be used in real technology, such as is the case with quantum computing. Finally, the theoretical predictions associated with entanglement are discussed in reference to two quantum optics experiments.

Table of Contents

II. INTRODUCTION

This thesis establishes a basic understanding of quantum entanglement by discussing three key topics: the mathematical formalism of quantum mechanics, the application of entanglement in technological systems such as quantum computing and the results of two quantum optics experiments which explore the interference effects of entangled two-photon systems. Discussing the theory of quantum entanglement in the context of these three separate topics will allow for the abstract qualities of entanglement to be continually explored and reinforced.

A. Theory of entanglement

Quantum entanglement, in this section, will be described in reference to theoretical optical experiments involving the polarization of light. To develop an intuitive understanding of such experiments and the strange implications of entangled systems, this section will outline the following subjects: the polarization state of light, how it can be expressed as quantum state, and the difference between a mixed state and an entangled state.

1. Polarization states

The first important concept that will be discussed in this section is the idea of light having a polarization state. Each electromagnetic wave of light has a polarization state that is defined by the direction of the wave's oscillating electric field and how that direction changes over time. It is also important to note that this direction, no matter how it may be changing, will always be in a plane perpendicular to the wave's direction of propagation. There are four different classifications of polarization that each account differently for a wave of light's changing electric field: linear, circular, elliptical, and random. The difference between these polarization types can be visualized more easily by identifying what is called the polarization vector.

(a) The polarization vector. The polarization vector is a unit vector that combines the directional components of a light wave's oscillating electric field and, in doing so, defines the polarization of the wave. To generate this vector, this paper will follow the logic laid out by the text of Beck[1] which starts by looking at general expression for the electric field of a light wave traveling in the z direction given by:

$$\vec{E} = E_x \vec{u}_x + E_y \vec{u}_y$$

The total field, $\vec{E}$, is broken up into x and y directional components, $\vec{u}_x$ and $\vec{u}_y$, that each have an associated magnitude represented by, E_x and E_y, respectively. The oscillatory nature of the electric field for both components can be observed more readily by expressing their magnitudes in cosine form:

$$E_x = E_{o_x} \cos(kz - \omega t)$$

$$E_y = E_{o_y} \cos(kz - \omega t + \varphi)$$

E_{o_x} and E_{o_y} are the amplitudes of oscillation for each component, z is the waves position and t is time. The two terms, k and ω, are two inherent properties of the wave known as the wave number and the angular frequency, and they can be found through the following relationships involving the wavelength, λ, frequency, f, and speed of light, c:

$$k = \frac{2\pi}{\lambda} = \frac{2\pi f}{c} = \frac{\omega}{c}$$

The last undefined term found in the two component expressions, φ, is a term that represents a possible phase shift which allows for the two components to oscillate out of phase from one another.

The components of the electric field, as expressed in their cosine forms, are intuitive to understand as they are real and describe an observable physical quantity. However, to generate

the polarization vector, it is more useful to think of these cosine terms as the real part of a

complex exponential which can be understood through Euler's formula:

$$e^{ix} = \cos(x) + i\sin(x)$$

Applying this general relationship allows for the components of the electric field to be rewritten

in terms of a complex exponential:

$$E_x = E_{o_x} e^{i(kz-\omega t)}$$

$$E_y = E_{o_y} e^{i(kz-\omega t+\varphi)}$$

The entire expression for the whole field can now be thought of in terms of these newly defined

components:

$$\vec{E} = E_{o_x} e^{i(kz-\omega t)} \vec{u}_x + E_{o_y} e^{i(kz-\omega t+\varphi)} \vec{u}_y$$

To get to the complete polarization vector, it is now necessary to rewrite this expression for the

field in terms of its full amplitude, E_o, instead of just the components. This amplitude can be

understood by applying the general relationship between any general vector and its components

which, in this case, can be expressed in the following way:

$$E_o = \sqrt{E_{o_x}^2 + E_{o_y}^2}$$

The expression for the electric field can now be written in terms of its complete amplitude:

$$\vec{E} = E_o e^{i(kz-\omega t)} \left[\frac{E_{o_x}}{E_o} \vec{u}_x + \frac{E_{o_y}}{E_o} e^{i\varphi} \vec{u}_y \right]$$

The expression in the brackets is defined as the polarization vector and it is associated with the

term $\vec{\varepsilon}$. This vector is a unit vector and, in its general form, is also complex when the phase shift

is positive. It provides information about the direction of the electric field as well as how a phase

shift between the field's components effects this direction. Having developed the idea of the

polarization vector it can now be used to understand the different polarization states.

(b) Linear polarization. Linear polarization can be understood most easily by looking at the polarization vector in the special case where there is no phase shift between the components of the electric field. If this is the case, then the complex term goes to one and the whole vector becomes real:

$$\varepsilon = \left[\frac{E_{0x}}{E_0} \vec{u}_x + \frac{E_{0y}}{E_0} \vec{u}_y \right]$$

This expression describes a single direction of oscillation that points in a straight line and thus is why this form of polarization is considered to be linear. The angle that this line makes with the respect to the x-axis, θ, can also be observed by implementing the simple trig relationship, tangent, which relates the two components:

$$\theta = tan^{-1} \left[\frac{E_{0y}}{E_{0x}} \right]$$

(c) Circular polarization. Circular polarization can be most easily observed by, once again, looking at a special case. This case will involve two specific changes to the polarization vector: a phase shift represented by setting $\varphi = \pi/2$, and setting the components of the field equal. Doing this generates the following relationship between the components of the fiend and the whole field:

$$E_{0y} = E_{0x} = \frac{E_0}{\sqrt{2}}.$$

Extrapolating these two changes to the polarization vector results in the following expression:

$$\varepsilon = \frac{1}{\sqrt{2}} (\vec{u}_x + i\vec{u}_y)$$

This vector, unlike the case of linear polarization, contains both real and complex parts which makes it more difficult to interpret. To understand what this equation means for the actual observed oscillation of the field it is possible to once again return to the original component

9

equations for the entire field as they were expressed using cosines. Subbing the phase shift and

the known amplitudes of oscillation into these two component equations allows for the real

oscillation of the field's components to be observed more easily:

$$E_x = \frac{E_o}{\sqrt{2}} \cos(kz - \omega t)$$

$$E_y = \frac{E_o}{\sqrt{2}} \cos\left(kz - \omega t + \frac{\pi}{2}\right) = -\frac{E_o}{\sqrt{2}} \sin(kz - \omega t)$$

These two expressions can now be interpreted by looking at how the components oscillate over

the course of one period, T, at a given position, z=0. When this is done, the following result is

generated:

$$E_x = \frac{E_o}{\sqrt{2}} \cos(-\omega t) = \frac{E_o}{\sqrt{2}} \cos(\omega t)$$

$$E_y = -\frac{E_o}{\sqrt{2}} \sin(-\omega t) = \frac{E_o}{\sqrt{2}} \sin(\omega t)$$
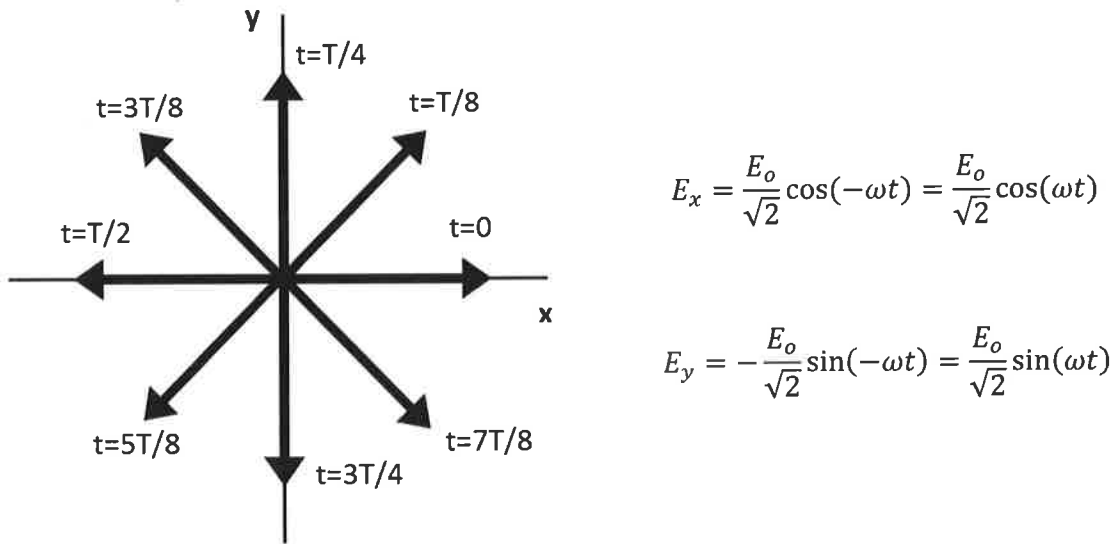
Figure 1: Original illustration of how the direction of the electric field changes for a left-circularly polarized wave with the corresponding component equations, inspired by figure 2.2 in Beck[1]

This figure illustrates how the components combine to generate the total electric field vector at

different times. As time progresses, the field vector rotates in the counter-clockwise direction

around an axis pointing perpendicular. By the time the field has gone through one oscillation

period it has also fully rotated around the circle and returned to pointing in the original direction

10

it was at t=0. This scenario has illustrated what left-circularly polarized light looks like. As it might be assumed, a similar but opposite form of circular polarization is right-circular which is associated with the field vector rotating in the clockwise direction.

(c) *Elliptical and random.* Elliptical and random polarizations essentially encompass all the other polarization states that cannot be categorized in either of the special cases of linear or circular. In the case of elliptical polarization, the polarization is still well defined by its x and y components and the phase shift between them, but this definition does not correlate with either of the specific parameters associated with linear or circular polarization. Random polarization, as its name would suggest, is associated with a wave whose polarization fluctuates randomly in time. When this form of polarization is observed, the wave is said to be unpolarized and the exact components of the fields oscillation cannot be directly observed.

To illustrate how polarization states are described in a quantum mechanical framework, the following section will focus mostly on examples of linearly polarized light as it is the most straightforward to work with.

2. Quantum states

Up until this point, this section has outlined the classical interpretation of the polarization of light. To understand how polarization states can be used to describe entangled systems, it is first necessary to represent polarization in the notation of quantum mechanics. There are three main components of quantum mechanical notation that are necessary to understand polarization as a quantum state: state vectors, inner products, and operators. Each of these will be discussed in reference to an individual photon and then extrapolated to two photon systems.

(a) *State vectors.* The different possible linear polarizations that were discussed previously are expressed in quantum mechanics by state vectors. How these state vectors are

11

used can be visualized most easily by thinking of two familiar linear polarizations: horizontal, $\theta=0$, and vertical, $\theta=90$ degrees. Each of these polarizations can be expressed as a state vector by using what is called Dirac notation. This notation involves the use of two different kinds of state vectors, bras and kets. Initially, it will be most useful to think in terms of kets exclusively. The general ket notation for an arbitrary quantum state is $|\psi\rangle$. For the specific cases of horizontal and vertically polarized light the ket notation is $|H\rangle$ and $|V\rangle$, respectively. Although it might seem obvious to compare these state vectors directly to the horizontal and vertical orientations of the classical polarization vector, it is important to note that these two types of vectors are not the same. The polarization vector has a physical representation and points in an observable direction. State vectors, on the other hand, exist in an abstract mathematical space called a Hilbert space and they don't point in any real observable direction. Although this distinction is difficult to interpret, it is still an important piece of information that distinguishes the quantum mechanical interpretation of polarization from the classical.

An important feature of state vectors is that they can be used to form a basis in which other polarization states can be represented. This new expression for a general polarization state is expressed as a linear combination of the two $|H\rangle$ and $|V\rangle$ state vectors:

$$|\psi\rangle = c_H|H\rangle + c_V|V\rangle$$

The coefficients in front of the state vectors here are complex numbers which are known as probability amplitudes. When squared, these amplitudes give the probability of observing the correlated basis state. Additionally, if the general state vector is said to be normalized then the sum of the generated probabilities must add up to 1; in other words, the sum of the squares of the complex coefficients must equal 1. This general form is useful as it can be used to describe any

polarization state. Table I illustrates how this general form can be used to illustrate a series of common polarization states:

Polarization State	General Expression in $|H\rangle$, $|V\rangle$ basis
$|H\rangle$	$|H\rangle$
$|V\rangle$	$|V\rangle$
$|+45\rangle$	$|+45\rangle = \frac{1}{\sqrt{2}}(|H\rangle + |V\rangle)$
$|-45\rangle$	$|-45\rangle = \frac{1}{\sqrt{2}}(|H\rangle - |V\rangle)$
$|L\rangle$ (left circular)	$|L\rangle = \frac{1}{\sqrt{2}}(|H\rangle + i|V\rangle)$
$|R\rangle$ (right circular)	$|R\rangle = \frac{1}{\sqrt{2}}(|H\rangle - i|V\rangle)$

Table I: Table of various polarization states and their corresponding expressions in Dirac notation, inspired by Table 3.2 in Beck[1]

The idea of creating a general basis state using a linear combination of horizontal and vertical state vectors can be extended to two particle systems as well.

(b) Type-I parametric downconversion and two-particle systems. To observe how two particle systems can be represented in the $|H\rangle$ $|V\rangle$ basis, this section will work through one of possible outcomes associated with a process called parametric downconversion which will be abbreviated as PD for the rest of this paper. PD is the process of spontaneously generating two photons from a single photon incident on a non-linear crystal [5]. It is a process which occurs in materials with birefringent properties such as a BBO (Beta Barium Borate) crystal. Birefringent materials are anisotropic, which means that they have multiple indices of refraction that depend

13

upon the polarization of the light passing through them relative to their optic axes [1]. The simplest form of birefringence, and the one most pertinent to this paper, occurs in uniaxial crystals. These crystals have a single optic axis which determines their anisotropic behavior. In a uniaxial crystal, light that is polarized perpendicular to the optic axis will experience an index of refraction, n_o, which is known as ordinary. Conversely, light polarized along the optic axis will experience a different index, n_e, which is known as extraordinary. The relationship between these two indices can be used to classify materials into two types of birefringence. If $n_o > n_e$ then the material is classified as being negatively birefringent. This means that light polarized along the extraordinary axis will travel through the material at a faster speed than light polarized along the ordinary axis. The reverse is true for positively birefringent materials where $n_o < n_e$. The axis associated with the lower index of refraction in a birefringent material, is often referred to as the fast axis.

Birefringent materials with a single optic axis, interacting with an extraordinary polarized incident pump photon, can generate two different types of PD, type-I and type-II, both of which result in the spontaneous generation of two output photons from a single input photon [5]. The two output photons are known as the signal and idler photon. Each of them has approximately twice the wavelength of the input photon and it is their relative polarizations that indicates the type of PD. If both photons emerge from the crystal polarized orthogonal to the pump photon, then it is called type-I. On the other hand, if the photons emerge from the crystal with one polarized along the ordinary axis and the other polarized along the extraordinary axis then this is considered type-II [5]. Following along with Beck[1]'s explanation of entanglement, we will initially only be looking at the case of type-I PD to develop and understanding of two-particle systems. This can be done by studying the following experimental setup in Figure 2:
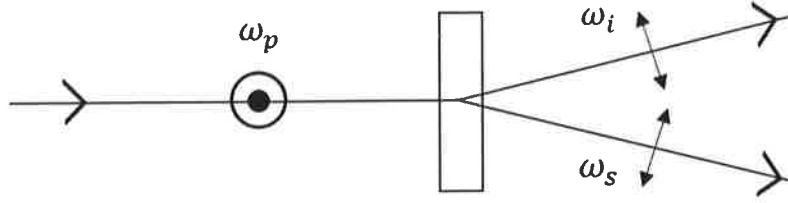
Figure 2: Original illustration of a single photon being split in two through the process of type-one parametric downconversion, inspired by the figure 8.1 in Beck[1]

In this setup, type-I PDC occurs when a single vertically polarized pump photon passes through a crystal. Both the signal and idler photons emerge from the crystal polarized orthogonal to the pump photon, which in this case means that they are horizontal. Additionally, they each have a new angular frequency associated with them: ω_i for the idler and ω_s for the signal. The two-photon system that is created in this example can be expressed as a direct product of the polarization states of the signal and idler photons:

$$|H\rangle_s \otimes |H\rangle_i = |H, H\rangle$$

This process can be done even if the polarization state of either the signal or idler photons are something other than vertical or horizontal. For instance, it is possible to place an optical element in the path of the signal photon that transforms its polarization state to be $|+45\rangle$. In this case the resultant two particle system could be expressed in a similar way by using the known general expression for a single photon polarized in the state $|+45\rangle$:

$$|+45\rangle_s \otimes |H\rangle_i = |+45, H\rangle = |+45\rangle = \frac{1}{\sqrt{2}}(|H\rangle_s + |V\rangle_s) \otimes |H\rangle_i$$

$$= \frac{1}{\sqrt{2}}(|H\rangle_s \otimes |H\rangle_i + |V\rangle_s \otimes |H\rangle_i)$$

$$= \frac{1}{\sqrt{2}}(|H, H\rangle + |V, H\rangle)$$

15

This sort of process can be replicated for any two-photon system with any combination of polarization states for the signal and idler photons. The result associated with this process is called a product state as it can be factorized into two separate states correlated with the individual particles. Product states are important for this paper as they indicate how ket vectors can be used to describe the state of an idler and signal photon simultaneously. However, neither mixed nor entangled states, although they are still two particle systems, can be written as product states. This intriguing characteristic will be discussed later, but for the time being it is important to understand product states as they are successful at introducing the fundamental concepts of two particle systems.

(b) *Inner product.* The next crucial topic that must be outlined is the inner product. To understand the inner product, the second half of the Dirac notation, bra state vectors, must now be introduced. Every ket state vector has a correlated bra state vector. For example, both ket vectors representing the H and V polarization states also have a corresponding bra state vector which is written in the following way: $\langle H|$ and $\langle V|$. Although this change may seem to be just notational, it can be understood in a more complex way when considering the fact that each state vector is associated with its own Hilbert space. Beck[1] explains the difference between the bra and ket vectors in light of this fact: "The vector space of bras is often referred to as the dual space to the vector space of kets." This idea can be understood to some degree by observing how a general ket state vector can be changed into the same basis but in bra form:

$$|\psi\rangle = c_H|H\rangle + c_V|V\rangle \quad \longleftrightarrow \quad \langle\psi| = c_H{}^*\langle H| + c_V{}^*\langle V|$$

This transition involves simply switch all the kets to bras while also taking the complex conjugate of each of the complex coefficients. Illustrating this not only shows how to change

between bras and kets, but also is helpful for understanding how they are inherently different and not just a change in notation.

Now that the bra state vector has been introduced, it can be used to understand the implications of the inner product. The inner product, like the direct product, is a mathematical operation used to combine state vectors. To form an inner product, a bra and a ket vector can be placed besides one another to form a bracket. This combination results in a scalar which is a complex number:

$$\langle \psi_1 | \psi_2 \rangle = c$$

Besides this general formula for an inner product there are two additional special results that will be especially important to understand for the calculations that will be done later. The first result is that the inner product of orthogonal vectors is equal to zero. This can be visualized most easily by taking the inner product of horizontal and vertical polarization state vectors:

$$\langle H | V \rangle = \langle V | H \rangle = 0$$

Additionally, the inner product of the bra and ket vectors of the same state will be equal to 1, so long as both state vectors are normalized. This, illustrated using horizontal and vertical polarization state vectors, looks like the following:

$$\langle H | H \rangle = \langle V | V \rangle = 1$$

The inner product can be extended to two particle systems rather easily as well. Taking the inner product of a two-particle system is essentially like taking the inner product of the bra and ket state vectors for the signal and idler photons individually:

$$\langle H, V | H, V \rangle = {}_s\langle H | H \rangle_s * {}_i\langle V | V \rangle_i = (1)(1) = 1$$

Or

$$\langle H, V | V, H \rangle = {}_s\langle H | V \rangle_s * {}_i\langle V | H \rangle_i = (0)(0) = 0$$

17

The last significant quality of the inner product is that it can be used to solve for the complex coefficients in the expression for a general polarization state. This ability will be illustrated by taking the inner product of $\langle H|\psi \rangle$ to solve for the complex coefficient in front of $|H\rangle$, which is c_H:
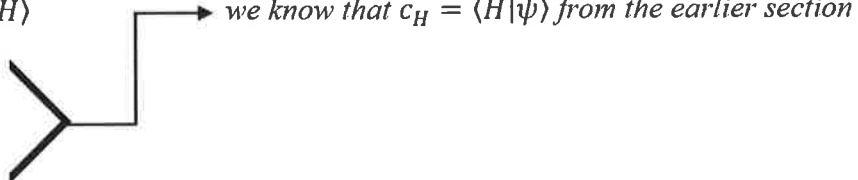
$$\langle H|\psi \rangle = \langle H|(c_H|H\rangle + c_V|V\rangle)$$

$$= c_H\langle H|H\rangle + c_V\langle H|V\rangle$$

$$= c_H(1) + c_V(0)$$

$$= c_H$$

Having outlined the functions of the inner product, this section can now move onto the last important tool necessary for understanding the difference between mixed and entangled states: the projection operator.

(c) The projection operator. The projection operator is used in this paper to calculate the probabilities of certain measurements of entangled two-photon systems. More generally the projection operator transforms a given input state, $|\psi\rangle$, into a separate output state with some probability. To understand this more specifically, this operator will be discussed in reference to an arbitrary optical element which transforms a general state, $|\psi\rangle$, into the $|H\rangle$ state with some probability. The previous statement can be illustrated by the following expression:

$$\hat{P}_H|\psi\rangle = c_H|H\rangle$$

If we assume that our general state is in the expected $|H\rangle |V\rangle$ basis, then we can work out what the projection operator, $\hat{P}_H$, will look like:

$$\hat{P}_H|\psi\rangle = c_H|H\rangle \qquad \longrightarrow \quad \textit{we know that } c_H = \langle H|\psi\rangle \textit{ from the earlier section}$$

$$= |H\rangle c_H$$

$$= |H\rangle\langle H|\psi\rangle$$

Having reached this equality, it is easy to see that:

$$\hat{P}_H = |H\rangle\langle H|$$

This specific result can be extrapolated to a more general expression for any projection operator:

$$\hat{P}_\psi = |\psi\rangle\langle\psi|$$

Moving forward from here, this paper can now make use of the notation developed in this section explore the strangeness associated with entangled states.

3. Entangled vs. mixed states

(a) Entangled states. To understand the difference between entangled and mixed states it is first important to define them individually. This can be done most efficiently by thinking about each of them separately in reference to the hypothetical experiment illustrated in Figure 3. The experiment depicted in Figure 3 is simply an extrapolation of the one previously observed in Figure 2, where now instead of having one BBO, we have two:
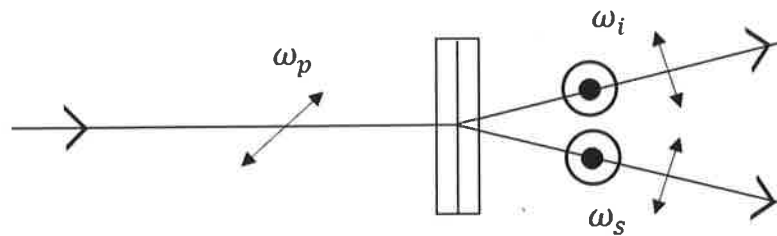
Figure 3: Original illustration of an experiment that uses two parametric downconversion crystals to generate entangled photons, inspired by Figure 8.2 in Beck[1]

The purpose of this experiment is to prepare a system of entangled photons. This is done by sending an input pump photon with a $|+45\rangle$ polarization state into two downconversion crystals who are positioned so that their optic axes are orthogonal: in this case aligned perpendicular to page and parallel to the page. Positioning the crystals in such a way ensures that they will

19

generate pairs of signal and idler photons with each pair being polarized orthogonally to the other. The first crystal will convert vertically polarized pump photons into horizontal signal and idler photons while the second crystal converts horizontally polarized pump photons into vertical signal and idler photons. Having the pump photon be polarized at $|{+}45\rangle$ makes each of these actions equally likely to occur. If the crystals are sufficiently thin, then it is impossible to know which crystal generated which photon. Additionally, it becomes impossible to determine the polarization of the signal and idler photons without making a measurement. If this level of indistinguishability is achieved, then the signal and idler photons can be said to be entangled. This means that the polarization state of this two-photon system exists as a superposition of the two possible states generated by the downconversion process and can be expressed in the following way:

$$|\phi^+\rangle = \frac{1}{\sqrt{2}}(|H,H\rangle + |V,V\rangle)$$

It is important to distinguish this expression from the result achieved through the direct product back in this paper's discussion of product state. The entangled expression does not allow for the individual $|H,H\rangle$ and $|V,V\rangle$ to be thought of as two separate states. More simply, the coefficient cannot be distributed to each individual ket vector. This is because the entangled state must be thought of as a single combined system of the two possible states of $|H,H\rangle$ and $|V,V\rangle$. The implications of this principle of superposition can be revealed by studying the probabilities associated with certain polarization measurements.

    The theoretical measurement that will be imposed on the previously prepared entangled state can be described by the following question: What is the probability that the signal photon is measured any polarization angle, θ_s, given that the idler was already measured at that same

angle, $\theta_i = \theta_s$? To answer this question, we must calculate a conditional probability. Beck[1] provides the following formula for a conditional probability:

$$P(\theta_s | \theta_i) = \frac{P(\theta_s, \theta_i)}{P(\theta_i)}$$

To calculate a value using this expression, it is necessary to separately calculate the numerator and the denominator. The numerator is a joint probability, which is equivalent to the probability of measuring the signal and idler photons at the same polarization angle. For an entangled state, this is calculated by finding the expectation value of the projection operator associated with the output state of our proposed system. An expectation value can be represented by the bra of the input state, the projection operator and the ket of the input state. Applying this logic, we can make the following calculation:

$$P(\theta_s, \theta_i) = \langle \phi^+ | \hat{P}_{\theta_s, \theta_i} | \phi^+ \rangle$$

$$= \frac{1}{\sqrt{2}} (\langle H, H | + \langle V, V |)(|\theta, \theta\rangle\langle\theta, \theta|) \frac{1}{\sqrt{2}} (|H, H\rangle + |V, V\rangle)$$

$$= \frac{1}{2} [(\langle H, H | \theta, \theta\rangle + \langle V, V | \theta, \theta\rangle)(\langle\theta, \theta | H, H\rangle + \langle\theta, \theta | V, V\rangle)]$$

$$= \frac{1}{2} [(cos\theta * cos\theta + sin\theta * sin\theta)(cos\theta * cos\theta + sin\theta * sin\theta)$$

$$= \frac{1}{2} [(cos^2\theta + sin^2\theta)(cos^2\theta + sin^2\theta)]$$

$$= \frac{1}{2} (1)(1) = \frac{1}{2}$$

The denominator can then be found similarly:

$$P(\theta_i) = \langle \phi^+ | \hat{P}_{\theta_i} | \phi^+ \rangle$$

$$= \frac{1}{\sqrt{2}} (\langle H,H| + \langle V,V|)(|\theta\rangle_i {}_i\langle\theta|) \frac{1}{\sqrt{2}} (|H,H\rangle + |V,V\rangle)$$

$$= \frac{1}{2}[({}_s\langle H| {}_i\langle H|\theta\rangle_i + {}_s\langle V| {}_i\langle V|\theta\rangle_i)({}_i\langle\theta|H\rangle_i |H\rangle_s + {}_i\langle\theta|V\rangle_i |V\rangle_s)]$$

$$= \frac{1}{2}[({}_s\langle H| * cos\theta + {}_s\langle V| * sin\theta)(cos\theta * |H\rangle_s + sin\theta * |V\rangle_s)$$

$$= \frac{1}{2}({}_s\langle H|H\rangle_s cos^2\theta + {}_s\langle H|V\rangle_s cos\theta sin\theta + {}_s\langle V|H\rangle_s cos\theta sin\theta + {}_s\langle V|V\rangle_s sin^2\theta)$$

$$= \frac{1}{2}((1)cos^2\theta + (0) + (0) + (1)sin^2\theta)$$

$$= \frac{1}{2}(1) = \frac{1}{2}$$

Having found both the numerator and the denominator, the total probability can be calculated:

$$P(\theta_s|\theta_i) = \frac{P(\theta_s, \theta_i)}{P(\theta_i)} = \frac{\frac{1}{2}}{\frac{1}{2}} = 1$$

What this result effectively means is that for photons prepared in the given entangled state, $|\phi^+\rangle$, if the idler photon is measured to be polarized at some angle, θ_i, then the signal photon will always be measured at that same polarization angle, $\theta_s = \theta_i$, no matter what the angle is. This is a unique result that doesn't appear to intuitively make sense. It is almost as though the two photons seemingly collude to always be measured at the same polarization angle. This strange result will now be shown to be unique to entanglement.

(b) *Mixed states.* Mixed states are different from entangled states in the sense that they do not maintain the idea that the general polarization state is a superposition of the two basis states. Instead, mixed states assume that the polarization is randomly prepared in either one of the two

possible states. This means that the polarization of a photon in this system is observed as being one state or the other, each having a separate probability of occurring. Mixed states also cannot be written as a product states, this is because they cannot be described by a single state vector. In order to compare a mixed state to the previously examined entangled state, this section of the paper will calculate the probability of the same measurement as before but instead of assuming a general entangled state, $|\phi^+\rangle$, it will assume that the two-photon system has been prepared with equal amounts of $|H, H\rangle$ and $|V, V\rangle$. Mixed state probability calculations rely on classical probability theory: A total probability is found by multiplying the probability of getting the desired result given one of the input states, together with the probability of that input state, summed over all the possible input states. Implementing this sort of calculation gives us the following results for the numerator of our probability expression:

$$P(\theta_s, \theta_i) = P(\theta_s, \theta_i || H, H\rangle) * P(|H, H\rangle) + P(\theta_s, \theta_i || V, V\rangle) * P(|V, V\rangle)$$

$$= \langle H, H | \hat{P}_{\theta_s, \theta_i} | H, H\rangle \left(\frac{1}{2}\right) + \langle V, V | \hat{P}_{\theta_s, \theta_i} | V, V\rangle \left(\frac{1}{2}\right)$$

$$= \frac{1}{2} (\langle H, H | \theta, \theta\rangle \langle \theta, \theta | H, H\rangle + \langle V, V | \theta, \theta\rangle \langle \theta, \theta | V, V\rangle)$$

$$= \frac{1}{2} [(cos\theta * cos\theta)(cos\theta * cos\theta) + (sin\theta * sin\theta)(sin\theta * sin\theta)]$$

$$= \frac{1}{2} (cos^4\theta + sin^4\theta)$$

A similar approach is necessary to find the denominator:

$$P(\theta_i) = P(\theta_i \| H, H\rangle) * P(|H, H\rangle) + P(\theta_i \| V, V\rangle) * P(|V, V\rangle)$$

$$= \langle H, H | \hat{P}_{\theta_i} | H, H \rangle \left(\frac{1}{2}\right) + \langle V, V | \hat{P}_{\theta_i} | V, V \rangle \left(\frac{1}{2}\right)$$

$$= \frac{1}{2} \left(\langle H, H | \theta \rangle_i \, _i\langle \theta | H, H \rangle + \langle V, V | \theta \rangle_i \, _i\langle \theta | V, V \rangle \right)$$

$$= \frac{1}{2} \left(\, _i\langle H | \theta \rangle_i \, _i\langle \theta | H \rangle_i \, _s\langle H | H \rangle_s + \, _i\langle V | \theta \rangle_i \, _i\langle \theta | V \rangle_i \, _s\langle V | V \rangle_s \right)$$

$$= \frac{1}{2} \left(cos^2\theta * (1) + sin^2\theta * (1) \right) = \frac{1}{2}(1) = \frac{1}{2}$$

Plugging the found numerator and denominators into the probability expression, a very interesting result can be observed:

$$P(\theta_s | \theta_i) = \frac{P(\theta_s, \theta_i)}{P(\theta_i)} = \frac{\frac{1}{2}(cos^4\theta + sin^4\theta)}{\frac{1}{2}} = (cos^4\theta + sin^4\theta)$$

This result indicates that a mixed will be able to generate the same results as an entangled state only if the measured angle of the idler photon is equal to either 0 or 90 degrees. For other measured polarization angles of the idler photon, such as 45 degrees, this result asserts that the signal photon will only be measured at the same angle half of the time. This result is vastly different from the result asserted by the entangled state calculations. The theory behind the unique correlation effects of entangled states, like the ones outlined in this section, will be used later in this paper to interpret the intereference effects being tested for in the two quantum optics experiments.

For now, however, the theory behind quantum states and entangled systems will be reinforced in a real world setting by looking at several examples of quantum computation.

III. APPLICATIONS OF ENTANGLEMENT

1. Qubits and quantum computing

Quantum computing is a new form of computing that utilizes quantum entanglement to create extremely fast and powerful computing systems. To develop an understanding of how quantum computing functions, this section will first build a theoretical model of the quantum bit, which is the fundamental system responsible for generating computing. Entanglement can then be introduced into the model through a discussion of various research articles that have explored different types of quantum bits and how they are applied in real computing systems.

(a) Classical computing and probabilistic bits. Quantum computation involves a lot of higher level mathematics and an understanding of complicated linear algebra systems. Taking this into account, this section will closely follow the theory described in work done by Kaye[7] et al. as it focuses less heavily on math and more on reinforcing the intuition we have already developed. A basic review of their work will be the basis for understanding the scientific journal articles whose research is pushing the boundaries of the field.

The quantum mechanical model of quantum computing will be built up in a similar way as the model of quantum states of polarization was developed in the first section: beginning in a classical framework and slowly transitioning to a quantum one. This is because a foundational understanding of classical computation is more intuitive and a lot of the math and logic associated with the classical model can be useful in understanding theory of quantum computation. Kaye[7] begins by developing a circuit model of computation which can be observed in Figure 4:
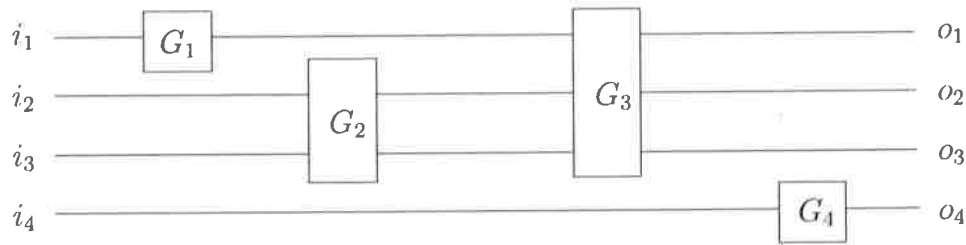
Figure 4: A circuit diagram with four wires. The i values are input bits, o values are output bits, and G boxes are gates which facilitate the transfer of information from an input wire to some output wire [7]

This model has four wires that run horizontally across the image and that pass through four gates that are labeled with capital G. These gates are responsible for the actual computation done by the circuit as they transfer input bits of information, displayed as i_n on the left, from one wire to another. Their presence in the circuit is what transforms the input data, i_n, into the output data on the right: the o_n values. The presence of gates also helps define the passing of time within this circuit model. A time slice is defined as the time taken to implement a single gate. Additionally, the number of time slices that exists in a circuit is defined as the depth. The other parameters used to describe this circuit model are space (width), which is the number of wires in the circuit. Space, depth, and the number of gates are the basic parameters for which circuits in this model are described. The specific model illustrated in Figure 4 is a circuit of depth 4, space 4 and a total of 4 gates. These values are a simple way of describing the complexity of any given circuit.

Kaye[7] pairs the basic modeling of a circuit with the mathematical description of computation for a classical system using vectors and matrices. To do this, focus is drawn to a single given point on a wire in the circuit for which a single bit of information can be observed. The state of the bit in a deterministic circuit is given as being either 1 or 0. To facilitate the move towards quantum computation, Kaye[7] instead develops the idea of a probabilistic circuit for which a single bit, at a given time, exists as a 2-dimensional vector of probabilities such that there are two terms, p_0 and p_1, that are used to describe the state of the bit at a given time [7]. In

26

this model, p_0 is the probability that the bit is in state 0 and p_1 is the probability that it is in state 1. Computation in this model requires that gates are understood as operators which transform the two-dimensional probability vectors into a new output state with some probability. This form should seem familiar as it mirrors the function of operators in quantum mechanical systems of polarization. A simple operator used by Kaye[7] to illustrate this idea is performed by a NOT gate which, in its most simple form, acts by flipping a deterministic bit from its given value of either 1 or 0 to the opposite value [7]. This operator is applied to probabilistic vectors by using a matrix that contains both possible input states of a state vector (0,1 and 1,0). The matrix itself is necessary in this case because the probabilistic state vectors effectively contain two possible inputs that need to be accounted for in the computation. Figure 5 illustrates how this NOT gate can lead to the flipping of the vector of probabilities by multiplying by the matrix with the state vector:

$$\mathrm{NOT} \begin{pmatrix} p_0 \\ p_1 \end{pmatrix} = \begin{bmatrix} 0 & 1 \\ 1 & 0 \end{bmatrix} \begin{pmatrix} p_1 \\ p_0 \end{pmatrix}$$

Figure 5: Illustration of the NOT gate flipping a probabilistic bit. NOT gate is a matrix of the possible inputs associated with a probabilistic bit [7]

The understanding of the probabilistic bit as a vector becomes very powerful when more than one wire is observed at a given time. Observing two wires inherently means observing two bits simultaneously. To successfully describe the state, in terms of probability, of these two bits requires the implementation of the tensor product. A tensor product allows for two vector spaces to be combined and is closely related to the direct product, which was used to combine individual polarization states into a two-photon system. The effect of the tensor product in the

current context is illustrated in Figure 6, where two probability vectors are combined to create a 4-dimensional vector of probabilities that describes the state of two bits at a given time.

$$\begin{pmatrix} p_0 q_0 \\ p_0 q_1 \\ p_1 q_0 \\ p_1 q_1 \end{pmatrix} = \begin{pmatrix} p_0 \\ p_1 \end{pmatrix} \otimes \begin{pmatrix} q_0 \\ q_1 \end{pmatrix}$$

Figure 6: The tensor product of two vectors describing the state of two bits in a circuit. Product is a 4-dimensional vector that describes the total system of two bits [7]

The 4-dimensional vector of probabilities outlines all the possible combinations of the two bits being observed at once. Understanding the formation of vectors such as these as well as what they represent is useful for understanding more complicated forms of computation in probabilistic settings. Developing this understanding of probabilistic classical bits and circuits lays the groundwork for developing the model of their quantum equivalents.

(b) Theory of quantum bits. Quantum bits, also known as qubits, are individual units of quantum information. The formation of a qubit mirrors the theory of a probabilistic classical bit. Like a classical bit, a quantum bit can be encoded into a system that contains two levels. Some systems that fall into this category are moving photons that can travel along one of two possible paths, spin ½ particles such as electrons, and even electrons bound between to two distinct energy levels [7]. Each of these systems, among others, allow for a state of 0 or 1 to be associated with an observed state of the system. In a classical system, probabilities of observing these states were given with the values of p_0 and p_1. As we know, in a quantum system, each state is associated with a complex coefficient, which is related to probability. In this case, the quantum state will be a linear combination of the basis states 0 and 1, each of which is associated with a complex coefficient a_0 and a_1. The entire system can be expressed as it is illustrated in Figure 7:

28

$$\alpha_0|0\rangle + \alpha_1|1\rangle$$

Figure 7: General state of a quantum bit with a_0 and a_1 being complex coefficients that are described as the amplitudes of each of the basis states, 0 and 1 [7]

This is the most simplified form of a qubit. Much like the quantum states associated with polarization, the basis states of 0 and 1 are associated with a Hilbert space. Combining them in this way allows for a single vector to be defined within the Hilbert space that is associated with state of the entire system. This complete vector form of a qubit is displayed in Figure 8. It is an extended version of the system displayed in Figure 7 and has the coefficients a_0 and a_1 written in their complex forms.

$$|\psi\rangle = \cos\left(\tfrac{\theta}{2}\right)|0\rangle + e^{i\varphi}\sin\left(\tfrac{\theta}{2}\right)|1\rangle$$

Figure 8: General vector form of a qubit [7]

The vector described by this system can be understood more thoroughly by building off the understanding of a classical bit. The state of classical deterministic bit can be equal to either 1 or 0. A probabilistic classical bit expands upon this system and can be described by a two-dimensional probability vector that contains the terms p_0 and p_1 which represent the probability of the bit being in either the 0 or 1 state. The vector form of a qubit can be described as a single point on a 3-dimnsional surface called a Bloch sphere [7]. All three bits and their interpretations can be observed in Figure 9.
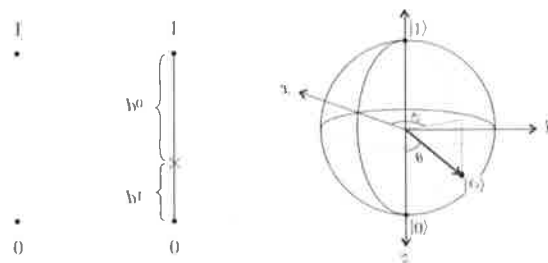

Figure 9: States of deterministic classical, probabilistic classical, and quantum bits [7]

Every point on the sphere corresponds to a pure state of the system. The two basis state vectors, 0 and 1, can be observed as the vectors pointing directly up and down on the z axis. The coefficients in front of the basis vectors determine the components of the entire state vector while the phase shift term, φ, rotates the vector around the sphere. Each state on the sphere, except for the pure states of 0 and 1, represents a superposition of the two basis states. This system allows for an infinite number of states to be generated compared to the classical bit who only has the two states 0 and 1. With the basic form of the qubit described it is now interesting to explore what natural phenomenon have been used to create them as well as how they can be used in computation.

(c) *Formation of real qubits.* As described before, any two-level system can be used as a qubit. Work done by Tosi[11] et al. illustrates how the outermost electron and nucleus of a phosphorus atom can be used as qubits. The electron itself is a two-state system that can be in either a spin up or down position. The alignment of electron is controlled by applying a magnetic field to the area surrounding it. The electron can then be flipped to the spin up state by applying a specific amount of energy to the electron in the form of a microwave pulse. The exact frequency of the microwave pulse is found by considering the magnetic field that the electron is placed within. With the magnetic field known, the resonance frequency of the electron can also be found. This frequency is what is applied to the electron to force it into the spin up state. Using different pulses of this frequency, the electron can be placed into different superpositions between the states of spin up and down. This setting is like the image of the Bloch sphere with the vector representing a pure state between the basis vectors 0 and 1. The nucleus of the same atom can also be used as qubit as it too has a spin associated with it. Reading out the values of the spin of both of these systems is done by placing the phosphorous atom within a silicon 28

transistor. It is also important to note that silicon 28 is necessary because it naturally does not have any nuclear spin. The lack of nuclear spin allows for the changes in the electron system associated with magnetic fields to be attributed solely to the experimental equipment and the phosphorous atom itself.

To observe the spin of the electron, Tosi[11] et al. observe changes in current flowing through the transistor. This is possible because the additional energy given to the phosphorous electron to put it in the spin up state is enough to kick the electron out of the atom and into the transistor leaving the phosphorous with a positive charge. The additional positive charge effectively increases the current flowing through the transistor and is used to indicate when the electron is in the spin up or down state. A similar technique is used to observe the spin of the nucleus as well as the small magnetic field produced by the nucleus plays a part in determining the resonant frequency of the electron. This means that depending on the spin of the nucleus, the electron will either react or not to the magnetic pulses applied to it. Transitive thinking allows for the change in the current read to additionally be used to read off the spin of the nucleus.

In addition to electrons and nuclei, work done by Fiorentino[6] et al. uses single photons as a qubit. They encode information onto the photon by taking advantage of two of its properties: the polarization and the angular momentum [6]. The two polarization states are simply defined as horizontal and vertical while the two momentum states are related to the photon's position within the beam and are defined as either top or bottom. Polarization and momentum states are created by implementing various forms of beamsplitters. To create the two polarization states, a device called a Sagnac interferometer is placed within the path of the beam. The interferometer has a prism that directs differently polarized light in two different directions, thus creating the two states. Additionally, the momentum states are separated by placing a halfwave plate with its optic

axis 45 degrees from vertical in the path of the photon beam. The photons essentially exist in a superposition of polarization and angular momentum states. Information can be read off of these formed qubits by sending them through an additional optical system which ends in two coincidence detectors that are located at the end of the split beams of photons.

Having provided a few examples of the formation of real qubits it is now interesting to understand how they can interact with gates and other qubits to generate computation.

(d) Quantum computation with entangled qubits. Computations can be done with qubits in a similar fashion as the previously explained classical bits. In both systems input bits interact with gates or operators to ultimately develop a different output value. In the qubit system, actions done to the bit by an operator correspond to rotations in the axes of the Bloch sphere [7]. This changes the output state of the system in a similar way that a NOT gate changes the state of the classical system.

Two bit systems in a quantum framework can also be acted upon by an operator to generate computations. The principle property of a pair of interacting qubits is their ability to become entangled. Entangled qubits exhibit similar properties to that of entangled photons: the state of one qubit cannot be described completely without considering the state of the entire quantum system. This means that the states of entangled qubits are inherently correlated with one another.

Having entangled qubits allows for more complex systems computing systems to be created. To read off the state of these highly entangled states in full, it is necessary to have more information to describe the entire system. This means that more information can inherently be encoded onto a system of qubits compared to classical bits. A simple comparison can be made by looking at two qubits versus two deterministic classical bits. To describe the system of two

deterministic quantum bits only two numbers are needed, 0 and 1. The two-qubit system, on the other hand, requires 4 complex coefficients to completely describe the system. Increasingly complex systems of entangled qubits require exponentially more numbers to describe them compared to classical bits. This translates to more potential opportunity for information to be encoded.

The application of qubits as a powerful new tool for computation has been implemented in select technologies, but the widespread use has been limited by the precision the settings required for qubits to exists. Many of the substances used to create qubits, such as electrons and photons can only be worked with in lab settings that aren't practical for everyday use. Electrons, for example, must be cooled to near absolute zero in order to be used as qubits as the thermal energy present at room temperatures will destroy the two-spin state system by providing the electron enough energy to constantly switch between states uncontrollably. Looking forward into the future, Boykin et al.[3] experiment with a process of algorithmic cooling in hopes that their findings will result in the creation of more efficient quantum computers. On a basic level, algorithmic cooling is a phenomenon in which certain forms of computation done with a quantum computer result in a negative entropy and thus a cooling effect. Their research is a breakthrough in the sense that the computation they have developed involves qubits interacting with their environment to naturally create a cooling effect. Outside of this research, interactions with the environment normally have a disruptive effect on the qubit system like in the case of thermal energy disrupting the spin states of an electron. Hopefully the work done by Boykin[3] will allow for qubits to be created and maintained more efficiently.

IV. EXPERIMENTS

1. Introduction and theory

To illustrate how entanglement can be observed in a lab setting, Dr. Caraher and I conducted two optical experiments with the intention of observing intereference effects previously studied in entangled photons systems.

(a) Type-II parametric downconversion. Type-II PD was desirable for our experimental setup because the entangled signal and idler photons are polarized orthogonal to one another. This characteristic allowed for us to manipulate the paths of the photons individually using optics that are sensitive to polarization. In type-II PD entanglement is generated in a different way than type-I. Catalano[5] provides a useful figure which illustrates an important characteristic of type-II PD:

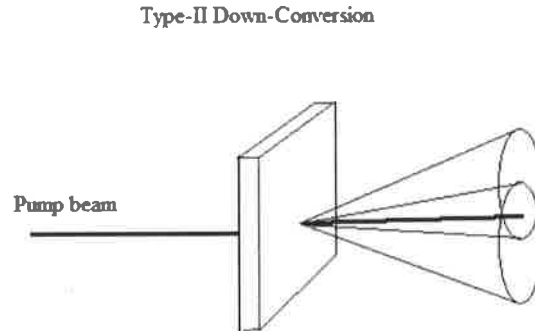**Type-II Down-Conversion**

Pump beam

Figure 10: Illustration of type-II parametric downconversion [5]

Figure 10 illustrates nicely how the output beams of type-II PD are constrained to be inside one of two cones. Each cone is associated with a certain polarization. Entanglement is observed only in the area in which the two cones intersect. This is because the polarization within that area is uncertain, and the state of the system must once again be described as a superposition of the possible polarization states. Additionally, it is important to note that there is an inherent $\delta\tau$

associated with type-II PD. This is caused by the birefringent nature of the uniaxial BBO crystal as discussed earlier. One of the downconverted photons will be polarized along the fast axis while the other is polarized perpendicular to it. This means that they will experience different indices of refraction, and thus will move through the material at different speeds. Newlight Photonics, the manufacturer of the BBO crystal used in this experiment, provided a calculated delay time of approximately 96.7 femtoseconds which was found by finding the speed of light along the fast and ordinary axes and generating a travel time for each photon based upon the thickness of the crystal. Uncertainty in this number is due to an uncertainty in where the photons were downconverted within the crystal.

(b) Hong-Ou-Mandel effect. The Hong-Ou-Mandel effect is an interference effect that can be observed when detecting coincidence rates of entangled photon pairs passing through a beamsplitter. Branning[4] illustrates a simple optical system which can generate such an effect:
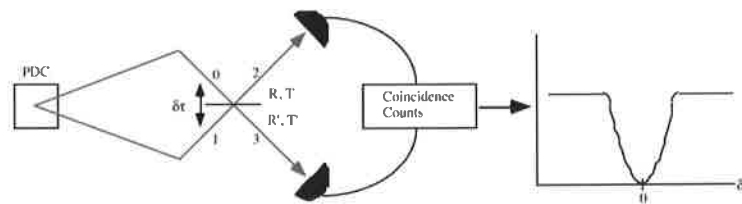

Figure 11: Simple representation of an optical system that generates the Hong-Ou-Mandel effect [4]

This system begins with a PD crystal which generates entangled signal and idler photon pairs whose individual paths are indicated by the red lines. These photons are sent through an undisclosed optical path so that they both come together at a beam splitter at the same time. The photons each have an equal chance to being either reflected or transmitted at the beam splitter. This means that there are generally four possible outcomes for the system: both are transmitted, both are reflected, the signal is reflected and the idler is transmitted, or the idler is reflected and

35

the signal is transmitted. A coincidence count is recorded when both detectors are hit with a photon within a certain collection time window. In the case where either the idler or signal photon is reflected and the other is transmitted, both photons will travel towards one detector and no coincidence will be registered. It is only when both photons are either transmitted or reflected that they will go to different detectors and a coincidence count will be recorded. Taking into consideration the possible outcomes for this system, it is reasonable to expect to observe a coincidence count fifty percent of the time as double reflection or transmission will statistically occur half of the time. However, if the beamsplitter is placed in such a position where it becomes impossible to tell if the coincidence count was the result of a double reflection or double transmission, destructive interference occurs and the observed coincidence count rate will go to zero. The position of the beamsplitter in this case is such that the time it takes for each photon to either be reflected or transmitted and travel to the detector is the same. This strange intereference effect can be observed in the plot provided by Branning in Figure 10. In this plot, coincidence counts are recorded as a function of the travel time difference between the two photons, which in this case is indicated by the term $\delta\tau$. When $\delta\tau$ is equal to zero the photons are indistinguishable and there is complete destructive intereference. However, as the beam splitter is moved away from this position, toward one detector or the other, the time it takes for a reflected photon and a transmitted photon to reach the detector becomes increasingly distinguishable. As $\delta\tau$ gets farther and farther away from zero, the photons become more and more distinguishable in time, the destructive intereference slowly goes away and the coincidence count rate returns to expected rate of fifty percent.

Having developed intuition about the Hong-Ou-Mandel effect and the reasoning behind

implementing type-II PD, it is now possible to move forward to a discussion of our experimental

setups.

2. General Setup

Both of our experimental setups were essentially identical, and only differed in the way

$\delta\tau$ was varied. To avoid repetition, this section will first go over the aspects of each setup that

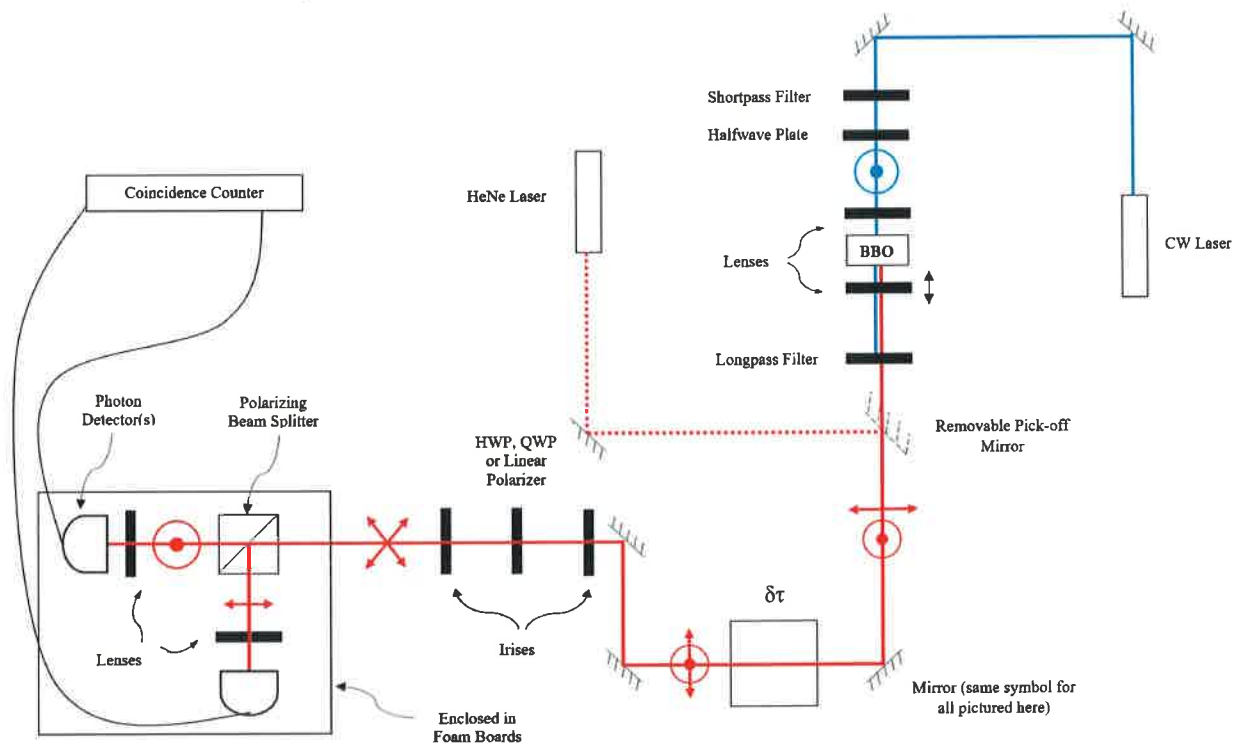remained constant in both experiments. These can be observed in the following Figure 12:

Figure 12: Original illustration of the complete optical system implemented in both of our experiments, with a general area labeled δτ to account for differences in the two

The setup beings with a continuous wave laser whose wavelength was measured using an

Oceanoptics spectrometer. Figure 13 illustrates the plot of intensity versus wavelength measured
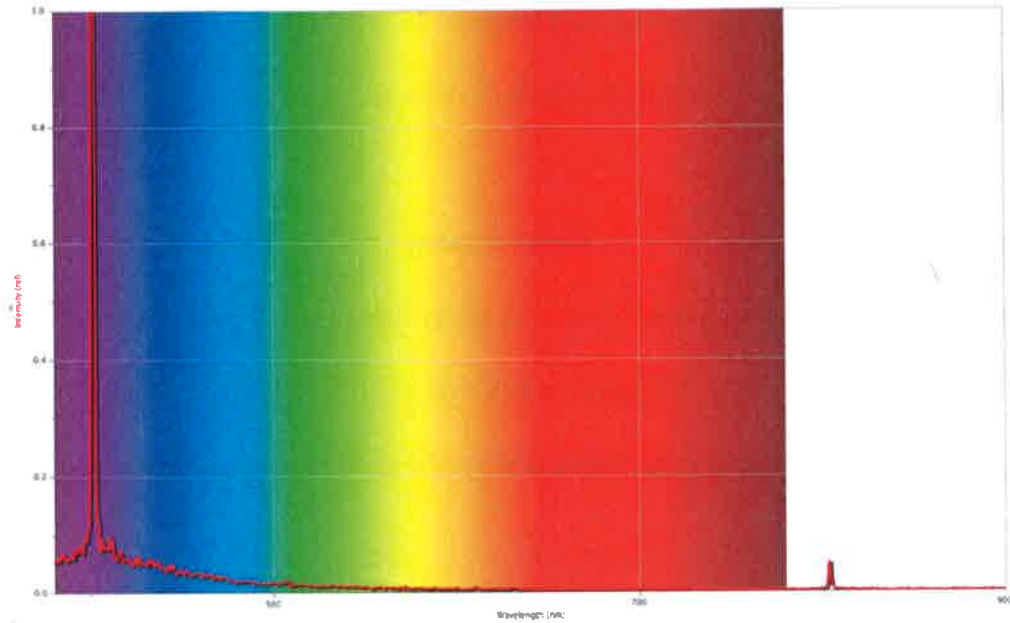
by the spectrometer for our laser:

Figure 13: Emission spectroscopy data collected for the CW laser used in both experiments

The main peak was measured to be at approximately 401.5 nm while the small peak was around

800 nm, although the exact measurement was not crucial. To avoid flooding our system with the

unwanted 800 nm light coming from the laser, the next optic we placed in the beam path was a

shortpass filter that transmitted light only of wavelength 400 +/- 40 nm. After being filtered, the

beam then passed through a halfwave plate so that the polarization of the blue beam could be

manipulated. In our final setup, the halfwave plate was oriented so that the polarization of the

beam would be vertical.

After passing through the halfwave plate the beam was then focused onto the BBO

crystal using an achromat lens which has a constant focal length regardless of the wavelength of

light being shone through it. The BBO crystal itself was placed in a gimble mount which allowed

for it to be rotated about its center in three different directions. This gave us control over the

alignment of the fast axis of the crystal so that we could align it correctly to the polarization of

the input light being controlled by orientation of the half wave plate. Having control over these

alignment variables helped us to create a system in which PD could take place. In our setup, we

aligned the BBO so that its fast axis was vertically oriented to match the input beam. Additionally, the small amount of delay caused by interaction of the birefringent BBO with the polarizations of the signal and idler photons is illustrated in Figure 12 by visibly separating the two photon symbols.

Both the downconverted beam and the extra blue light were then collimated by a second achromat lens which was mounted on a translation stage so that collimation could be optimized by small adjustments in the distance between the lens and the BBO. The original blue beam was then blocked using a longpass filter which only transmitted light of wavelength longer than 750 nm. This optic ensured that only our downconverted beam would be a part of the system.

At this point, the downconverted beam was steered into the unique optical system responsible for controlling the time delay between the signal and idler photons. In Figure 12, this is simply denoted as box $\delta\tau$. Details about the contents of this area for each setup will be discussed specifically in reference to the experiment in which they were used.

After passing through box $\delta\tau$, the beam was then steered with mirrors so that it would fly through two irises, whose height was determined by the height of the detectors. These irises were useful for aligning the beam as they indicated the path that the beam needed to follow so that the photons would be focused correctly onto the detectors. Additionally, their adjustable aperture size was helpful for controlling the amount of light passing into the final parts of the system. In between the irises was also a mount used to place a variety of optics such as halfwave plates, quarterwave plates and linear polarizers. This open mount provided us with the flexibility to manipulate the beam in a variety of different ways before passing it on through the final set of optics.

The last system of optics was enclosed in a box made of foam boards. Enclosing this system was important as it eliminated a significant amount of ambient light that would have disturbed the count values registered by the detectors. The contents of this light tight box can be observed in Figure 14:
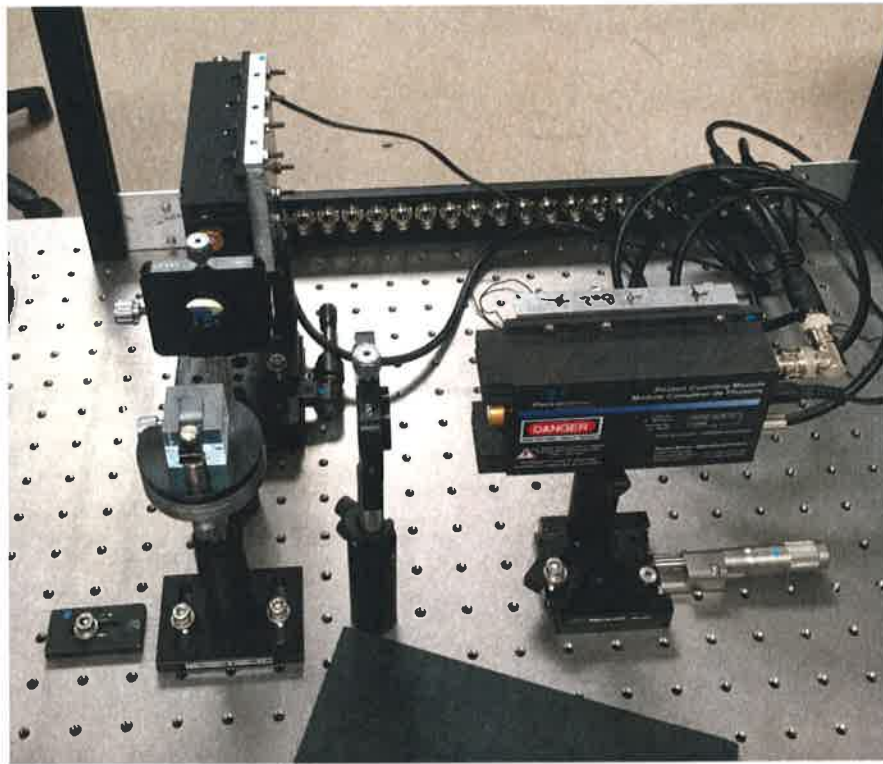

Figure 14: Image of the optical system used for detection of coincidence rates in both experiments

Once inside this box, the beam then passed through a polarizing beamsplitter cube, which transmits either horizontal or vertical light and reflects the other. The split beams were then each focused onto a detector using a best form lens which corrects for a different form of aberration called spherical aberration. Spherical aberration is the improper focusing of light that occurs due to the structure of the glass in a lens. Using these helped us achieve higher precision when focusing the downconverted beam on the detectors.

Count data was recorded by connecting the detectors to an Altera DE2 development and education board which was used to set the coincidence resolution. This is the maximum amount

of time difference between single detections that is still registered as a coincidence. In both of our experiments this was set to 7.05 +/- 0.09 nanoseconds. Count data was then collected using a program called LabVIEW which utilizes programable virtual instruments to display and record count data from the DE2 board.

The last element in our setup was a HeNe, helium neon, laser which was used purely for alignment purposes. Downconverted light from our previously discussed system was infrared and invisible to the naked eye. Matching the path of the visible HeNe laser to the path of the blue beam allowed us to visibly approximate the path of the downconverted light. Although the paths of the HeNe beam and the downconverted beam were most certainly not perfectly aligned, implementing this strategy allowed us to get everything close enough so that the final alignment could be optimized using readings from the detectors. The HeNe beam was introduced to the system using two steering mirrors, one of which was a removable pick-off mirror that was placed in the system when the visible laser was needed.

3. Experiment 1: Michelson interferometer

(a) Setup. The first experiment used an optical system called a Michelson interferometer to generate delay between the signal and idler photons. Figure 15 illustrates the different elements of the Michelson used in this experiment:
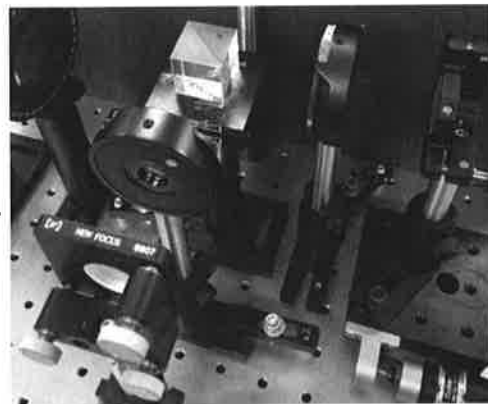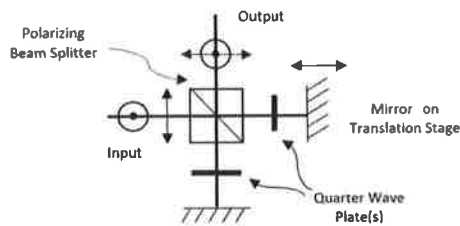

Figure 15: Original illustration of the Michelson interferometer used in experiment 1 alongside a real image of the system

41

The input photons enter the system with some $\delta\tau$ associated with type-II PD. They pass through a polarizing beam splitter and one is reflected and the other is transmitted, much like the system used to send the beams to the detectors. The two photons then each pass through a quarter wave plate which results in them becoming circularly polarized. After reflecting off of a mirror, the photons once again pass through the quarterwave plate and become linearly polarized once again. The process of passing through the quarterwave plate twice results in the linear polarization being rotated 90 degrees. This means that each photon will interact with the polarizing beamsplitter cube in the opposite way that it did the first time. The result of this system is that the both photons emerge from output port of the beamsplitter cube polarized orthogonally to one on another just as they were before. Time delay between the two photons is generated in this system by placing one of the mirrors on a translation stage so that its position relative to the cube can be controlled. Changing this distance alters the time it takes for one of the photons to travel through the system, thus ultimately changing $\delta\tau$. In our setup, we used a translation stage powered by a ZABER motor which allowed us to make controlled adjustments in the position of the mirror on the order of microns.

The last crucial part of this setup involved placing at halfwave plate oriented with its fast axis 22.5 degrees away from vertical in the open mount between the two irises leading into the detector box. This optic rotated the polarizations of both the signal and idler photons by 45 degrees so that it became uncertain how each photon would interact with the polarizing beamsplitter cube. In theory, generating indistinguishable photons pairs in this way would lead to destructive interference and a dip in coincidence counts similar to what was illustrated in Branning[4]'s thesis.

(b) Data and analysis. The ZABER motor utilized in the Michelson was compatible with the LabVIEW virtual instrument TauScan3.vi programmed by Dr. Caraher. This instrument recorded the counts registered for each detector, coincidence rates and delay times while simultaneously controlling the position of the motor. To collect data, we set the program so that it would place the mirror at a starting location far away from the cube and record count rates for half of a second at each position of the mirror. After each collection, the ZABER would then translate the mirror one step forward until it reached a target end position. Before discussing the data being presented in this section, there are two important distinctions that must be made: the difference between delay and $\delta\tau$, and the difference between the raw coincidence rate and the real coincidence rate.

$\delta\tau$ is the relative delay between the signal and idler photons, and when it is equal to zero this indicates that the photons are on top of one another. In Figures 16 and 17, delay represents the time difference between the two arms of the Michelson. The initial position of the mirrors in the Michelson at the start of the data run is associated with delay equal to zero. Every step of the mirror in the translating arm increases the delay parameter by an amount determined by the size of the translation. For both data runs, each step of the motor was associated with a 10 femtosecond increase in delay. Collecting data in this way was useful because we did not know the position of the translating mirror that was correlated with $\delta\tau$ equal to zero. In sweeping through a wide range of mirror positions we hoped to observe a dip in coincidences due to the Hong-Ou-Mandel effect. The delay time associated with the center of this dip would allow for us to identify the position of the translating mirror correlated with $\delta\tau$ equal to zero.

Figure 16(a) includes both the raw and real coincidence rates to illustrate the difference between the two. The raw coincidence rate, as indicated by the orange series, is the number of

simultaneous detections registered by the two detectors. This value contains within it a certain number of expected random coincidence counts that will occur simply due to the volume of photons hitting the detector and the size of the coincidence resolution. An estimate for the expected random coincidences per second can be generated by multiplying the individual count rates per second and the coincidence resolution time together. This expected random per second rate can then be used to determine a value for the total number of expected coincidences by multiplying by the collection time. The real rate of coincidences is indicative of downconverted photons hitting the detectors at the same time and can be found by subtracting the calculated number of randoms from the total recorded coincidence rate. All figures discussed in this paper, aside from 16(a), will display only real coincidence rates because the interference effects we are interested in do not affect the random coincidence rate.

Figures 16 and 17 display the results from two separate data runs. Each figure contains two graphs, a and b, which plot real coincidence count rates versus delay and the detection rates for the individual detectors versus delay respectively:
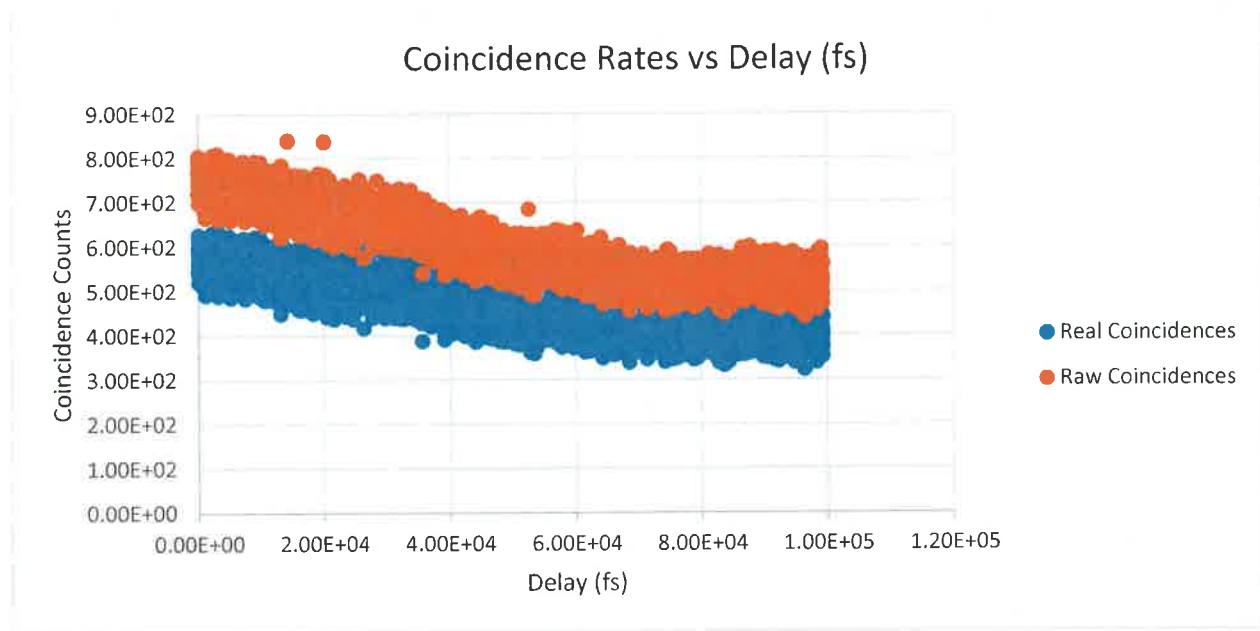

Figure 16(a): Both the raw and calculated real coincidence rates versus delay in femtoseconds
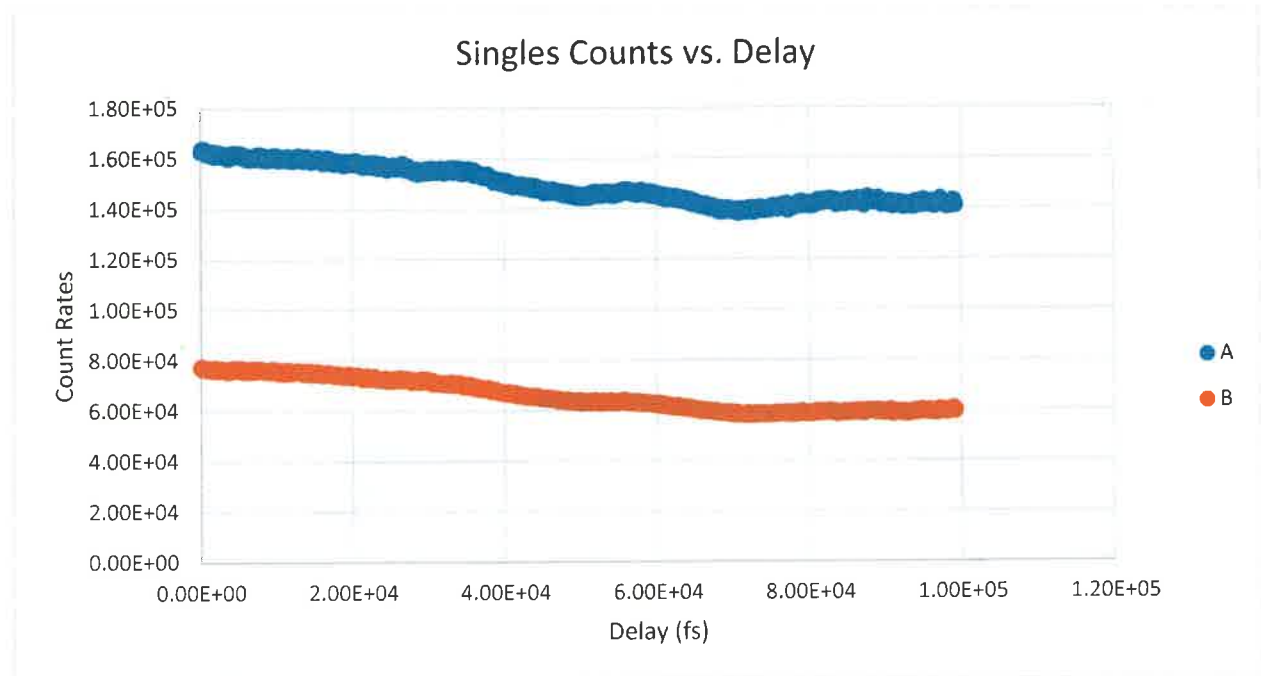
44

Figure 16(b): Count rates for individual detectors A and B vs delay in femtoseconds

Looking at the real coincidence rate versus delay in Figure 16(a) we do not observe a dip

in the real coincidence count rate correlated with the Hong-Ou-Mandel effect. This could be for

several reasons. The mutual downward trend in all the count rates indicated alignment issues in

the translating arm of the Michelson. Any alignment issue present in the mirror at the start of

collection would only be exacerbated by moving the mirror. Translating the misaligned mirror

could have steered the downconverted beam away from the desired beam path and resulted in the

decrease in count values. The striking difference in singles count values also indicated a possible

issue with the alignment of the optics in the detector box. It was possible that lens focusing the

beam onto detector B was improperly aligned, resulting in the large difference in counts

registered compared to A. Attempting to fix alignment issues in the detector box was a difficult

task because it required making adjustments inside the box while the detectors were on and

registering counts. Doing this increased the risk for the detectors to be exposed to large enough

amounts of room light to damage or even destroy them. To avoid this risk, we opted to first test

to see if the issue was a result of faulty electronics. This was done by switching the cables

connecting the detectors to the DE2 board for the next data run to see if the ratio between counts

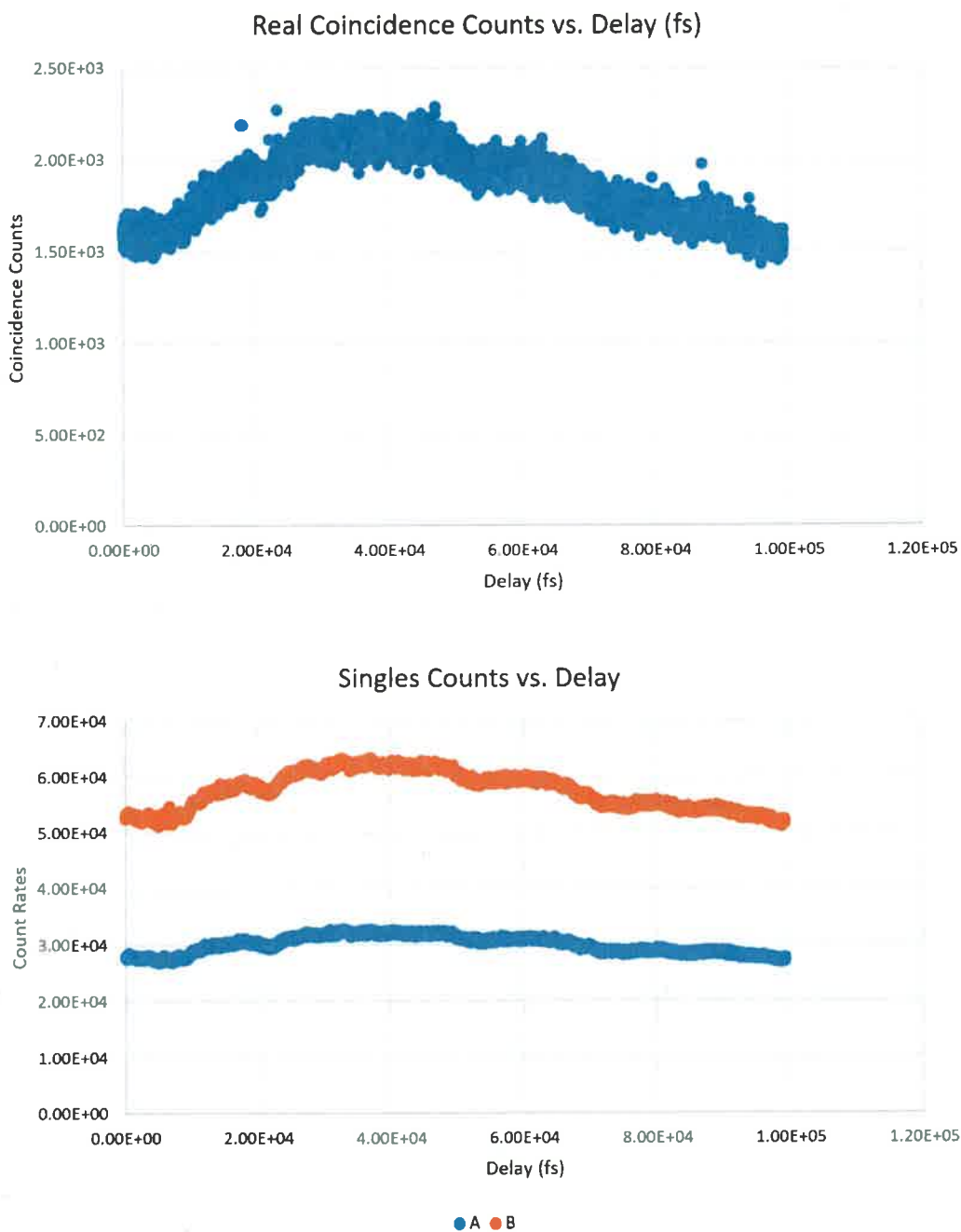in A and B persisted in both runs.

Figure 17: Data collected from our first run using the Michelson setup: plots coincidence rates vs. delay in femtoseconds (top), plots count rates for individual detectors vs delay in femtoseconds (bottom)

46

Before starting the second data run, the system was realigned in an attempt to get rid of the issues that may have been present in the first run. This was done by maximizing the raw coincidence rate through the adjustment of the orientation of the BBO, the position of the translating lens immediately after the BBO, the steering mirrors and the mirrors in the arms of the Michelson. The alignment of the translating mirror in the Michelson was tested by watching the count rates update while manually moving the mirror through its full range of positions. Additionally, the apertures of the two irises leading into the detector box were closed down farther in order to more precisely define the beam path.

Despite these adjustments the data collected in this similarly did not produced the desired Hong-Ou-Mandel effect. The peaked trend in the real coincidence count rate indicated more alignment issues with the translating arm of the Michelson. Additionally, the ratio of counts between A and B remained the same compared to the first run, indicating that the difference in the registered counts was not an electronic issue. The continual alignment issues stemming from the precise nature of the Michelson led us to try a different optical setup to control $\delta\tau$.

4. Experiment 2: quartz plates

(a) Setup. The optical system that we used to control $\delta\tau$ in our second experiment consisted of a series of positive birefringent quartz crystal plates similar to the system implemented by Sergienko[10]. Each plate was marked on the edges to indicate the direction of the optic axis. For each of the plates the optic axis was parallel to the marked edges. Being able to distinguish between the orientations of the plates was essential as it allowed us to align the optic axes of multiple plates to one another. Figure 18 provides an image of the quartz plates with their markings as well as the system used to mount them in the beam path:
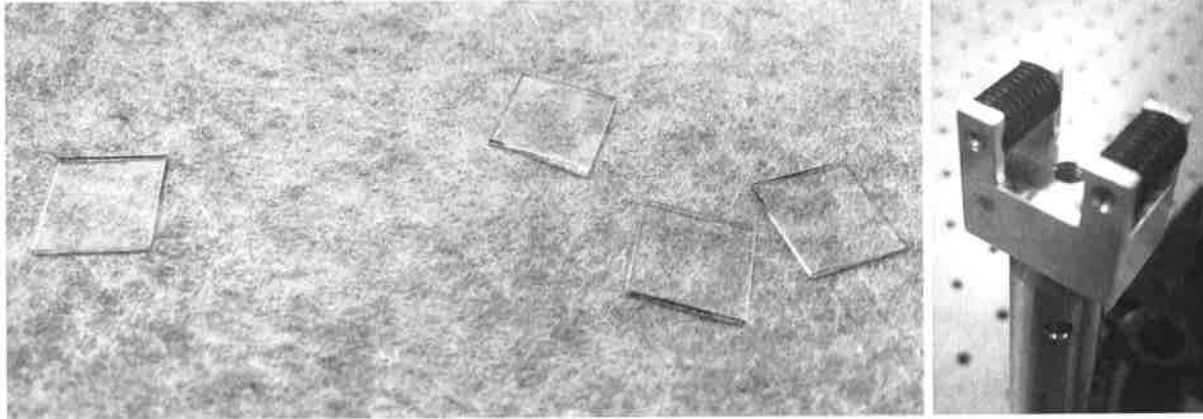
Figure 18: Birefringent quartz plates used to generate delay in experiment 2 alongside the instrument used to mount them

Unlike the BBO, the amount of delay correlated with each crystal plate was not provided by the manufacturer. To calculate this value, we found the speed of light associated with both the ordinary and extraordinary photons and converted it to a travel time based upon the distance traveled through the thickness of the crystal. The difference between these travel times was used as our estimated delay for each plate.

To correctly calculate delay, we had to account for the difference between phase velocity and group velocity. The difference between the two can be understood by looking at Figure 19:
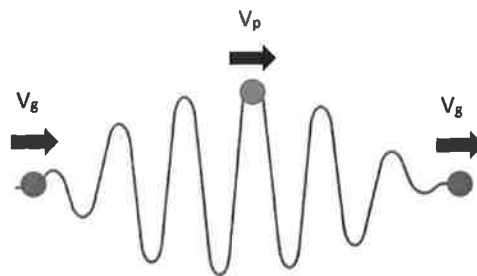

Figure 19: Illustration of photon propagating to the right with blue dots moving at group velocity and red dot moving at phase velocity

Figure 19 illustrates a photon that is propagating to the right. The blue dots define the boundaries of the envelope of the wave packet while the red dot is fixed to an arbitrary peak propagating inside the wave packet. The propagation speed of the entire envelope, as defined by the blue dots, is known as the group velocity and it is labeled in the Figure as V_g. This speed can be

different than the propagation speed of the individual peaks inside the wave packet, which is known as the phase velocity, V_p. Essentially this means that the red dot fixed to the peak can eventually overtake the blue dot on the right as the wave packet propagates to the right. When calculating the delay for each quartz crystal we were interested in the group velocity and not the phase velocity. This is because our system relies on manipulating the travel speed of photons, which are wave packets. Taking this into account, the following formula could be applied to calculate the group velocity of a photon with wavelength, λ_0, traveling through a medium with a given index of refraction, n, where c is the speed of light in meters per second:

$$v_g = \frac{c}{n - \lambda_0 \frac{\partial n}{\partial \lambda_0}}$$

Before we could utilize this formula, however, we first had to find the values of the indices of refraction associated with the ordinary and extraordinary axes and the value of the differential term $\delta n/\delta \lambda_0$. These terms were found using the following sellmeier equations for crystal quartz provided by Boston Piezo-Optics Inc.[2]:

(λ in μm)

$$n_0^2 = 3.4269 + \left[\frac{1.0654 * 10^{-2}}{\lambda - 0.010627}\right] + \left[\frac{0.00276113}{\lambda - .000974}\right] + \left[\frac{127.2}{\lambda - 108}\right]$$

$$n_e^2 = 3.5612557 + \left[\frac{.00844614}{\lambda - 0.0127493}\right] + \left[\frac{0.00276113}{\lambda - .000974}\right] + \left[\frac{127.2}{\lambda - 108}\right]$$

Using these equations generated the following values for n_o and n_e given the wavelength of the downconverted beam was estimated to be 803 nm:

$$n_0(.803\mu m) = 1.502394093$$

$$n_e(.803\mu m) = 1.545569781$$

These values seem to make intuitive sense since crystal quartz is positively birefringent.

To avoid having to differentiate the sellmeier equations, the differential term $\delta n/\delta\lambda_0$ for both axes was estimated by calculating $\Delta n/\Delta \lambda_0$ where:

$$\Delta n = n(\lambda_2) - n(\lambda_1) \quad \text{and} \quad \Delta\lambda_0 = \lambda_2 - \lambda_1$$

The values of λ_2 and λ_1 were selected to be 808 nm and 798 nm respectively. These values corresponded to either adding or subtracting 5 nm from the estimated wavelength of the downconverted beam. Plugging in these values into the sellmeier equations generated the following values for $\Delta n/\Delta \lambda_0$ for the two axes:

$$\frac{\Delta n_o}{\Delta\lambda} = \frac{n_0(.808\mu m) - n_0(.798\mu m)}{.808\mu m - .798\mu m} = 0.010760014$$

$$\frac{\Delta n_e}{\Delta\lambda} = \frac{n_e(.808\mu m) - n_e(.798\mu m)}{.808\mu m - .798\mu m} = 0.009345185$$

Having found these all of the necessary values, the group velocities could then be calculated for each axis:

$$n_0: \quad V_g = 2.01 * 10^8$$
$$\text{(in m/s)}$$
$$n_e: \quad V_g = 1.95 * 10^8$$

Taking into account the thickness of each plate being approximately .5 mm these group velocities generated and estimated delay time of 73.9 femtoseconds per plate.

(b) *Data and analysis.* Data in this experiment was collected using a simpler LabVIEW virtual instrument which recorded both the counts registered for each detector and the coincidences given a variable collection time. Each data run consisted of nine data points that were generated by cycling the four quartz plates in and out of the beam path at different orientations in the following order:

V4, V3, V2, V1, 0, H1, H2, H3, H4

In this notation, the H or V indicates the orientation of a crystal in regards to its optic axis, while the number 0-4 indicates the number of plates included in the system at that orientation.

The small number of data points in this experimental setup meant that several data runs could be completed in the time it took for one Michelson experiment run. This increase in collection efficiency gave us more time to run two additional tests on top of using a halfwave plate to look for a Hong-Ou-Mandel dip. The first new test involved placing a linear polarizer, set at 45 degrees, in the beam path to test for the constructive intereference effect observed by Kwiat et al.[8], while the second involved testing to see if placing quarterwave plate aligned vertically would have on the coincidence rate. Both coincidence rates and single detector rates were recorded for each of the nine crystal systems paired with each of the three optics. Additionally, a data set was recorded with no optic placed in the beam path in order to observe the effect that quartz plates themselves had on the count rates. Collections times were varied for each optic to make sure that a substantial number of counts were recorded for each. This was especially significant for the linear polarizer, as it transmitted substantially less light than the other two optics.

Unlike the Michelson experiment, real coincidence rates could be plotted against $\delta\tau$, as both the input delay of the photons coming from the BBO and the delay associated with individual quartz plates were known values. Figure 20 plots the recorded real coincidence rate versus $\delta\tau$ for each optic and the case of no optic:
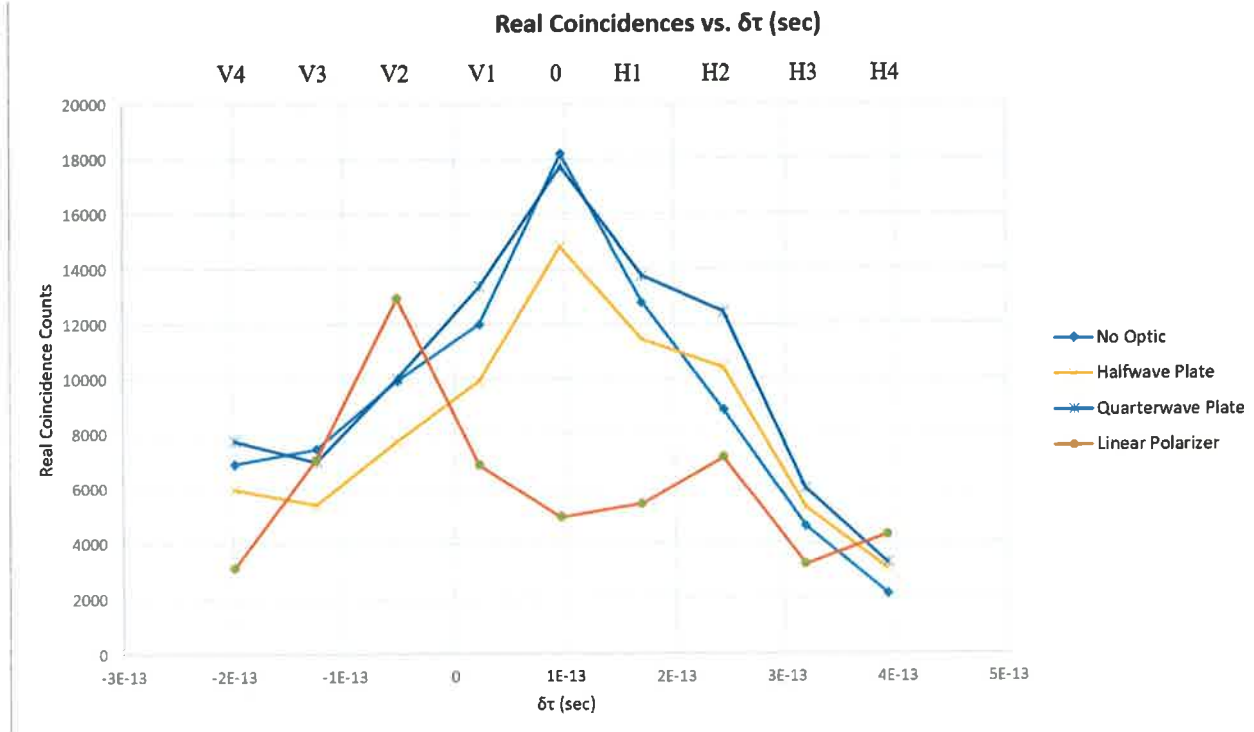
Figure 20: Plot of real coincidence counts versus delay between the signal and idler photons in seconds for the case of no optic, a HWP, QWP and Linear Polarizer

The data displayed in Figure 20, unfortunately, also does not show signs of much success. Trends in the halfwave plate data show no signs of the Hong-Ou-Mandel effect, while the trend in the quarterwave plate seems to mirror the baseline trend, revealing almost nothing about its effect on the coincidence rate. The data associated with the linear polarizer did see approximately a doubling of counts near $\delta\tau$ equal to zero, however, this is hard to take seriously given the low number of counts and the variance in the other data points. Failure to observe the desired interference effects could possibly have resulted from the poor quality of quartz plates themselves. Examining the trend in the baseline count rate indicates that the plates themselves do have a significantly negative effect on the coincidence count rates which is undesirable.

5. Discussion and conclusions

Unfortunately, neither of the experiments run in this paper allowed for the interference effects of entanglement to be directly observed. The Michelson experiment was disturbed by alignment issues both in the Michelson itself and in the detection system. Given more time to revisit this experiment I would spend more time on the alignment of both of those systems.

To ensure that the sensitivity difference in the two detectors was not the result of misalignment, I would attempt to translate the best form lens focusing the beam onto the detector registering less counts, while watching live updates of the count rates. Doing this would allow me to both test for and fix any alignment issues that may have caused the observed sensitivity issues.

To align the Michelson correctly, I would shine a white light source into the input port of the Michelson and manually translate the mirror using the ZABER until I observed an interference pattern displayed at the output port. Utilizing a white light source for alignment is helpful in this case because it has a very short coherence length. This means that the path length difference between the arms of the Michelson must be extremely small to produce interference effects. Aligning the Michelson in this way would allow for $\delta\tau$ equal to zero to be found much more quickly without having to sweep through the entire range of possible mirror positions. Lessening the amount of mirror translations per data run would substantially cut down on the total length of the data runs which would allow for more tests to be run more quickly. This could allow for the effects of the quantum eraser and the inclusion of a quarterwave plate in the optical system to be examined more readily.

The quartz plate experiment seemed to be disturbed by the plates themselves. I do not see any direct way to improve the setup implemented in this paper besides making similar

improvements in the alignment of the detector box. Additionally, I find the Michelson experiment more worthwhile to pursue as it provides a higher quantity of data as well as a higher level of precision when attempting to measure the desired intereference effects.

Assuming that our experimental setup could be aligned properly using the Michelson interferometer, it would also be interesting to investigate more thoroughly the role of indistinguishability on the interference of entangled photons by implementing a more complex delay system like the one used by Pittman[9] et al. Doing so would allow for our system to illustrate that two-photon interference effects can occur even if the path lengths of the interferometer are different and the photons arrive at the beamsplitter at different times.

V. CONCLUSION AND REFLECTION

This thesis has emphasized three important characteristics of quantum entanglement: how it is described using the mathematical formalism of quantum mechanics, how it can be applied to generate more efficient forms of computing and how it can be observed in the lab through quantum optical experiments. These three topics were selected together as their collective subject matter allowed for a strong theoretical framework of entanglement to be built while simultaneously reinforcing difficult concepts through concrete and intuitive examples.

This project represents everything that I have learned about quantum mechanics. Before starting this project, I had never opened a quantum mechanics textbook and I had never set foot in a quantum optics lab. Now, having finished this project I feel confident in my ability to understand the mathematical formalism associated with quantum entanglement to the degree that it is discussed in this paper. I also feel like I have developed a sense for working in an optics lab. I have learned how to align lasers to one another, how to use steering mirrors, how to align a Michelson interferometer and many other skills that have become more natural due to the

amount of time I spent working in the lab. Hopefully this paper has illustrated the skillset that I have developed over the past several months and can be useful for anyone attempting to develop a basic understanding of quantum entanglement.

VI. ACKNOWLEDGMENTS

I would like to first acknowledge and thank my entire committee for the time and effort they dedicated to supporting me during this thesis process. I especially would like to thank Dr. Caraher for putting in the time and effort, not only to sponsor this thesis, but also to help me build and run a real quantum optics experiment from start to finish. Before this project I had zero experience both in the lab, and in the field of quantum mechanics. Without his wisdom and guidance, this project would never have been possible.

I would also like to thank my family, girlfriend and friends for supporting me through the stressful parts of the project. Your support helped me push through the failures and realize the value of my work.

VII. REFERENCES

[1] Beck, Mark. *Quantum mechanics theory and experiment*. (Oxford University Press Inc., New York, 2012)

[2] Boston Piezo-Optics Inc. (April, 2017). *Crystal Quartz*. Retrieved from BPO Inc. website: http://www.bostonpiezooptics.com/crystal-quartz

[3] Boykin, P., Oscar, T., Vwani, R., Farrokh, V., and Rutger V. Proceedings of the National Academy of Sciences PNAS **99**, 6 (2002)

[4] Branning, David. Doctor of Philsophy in Physics, University of Rochester, 1998

[5] Catalano, Jesse. Bachelor of Science in University Honors and Physics, Portland State University, 2014

[6] Fiorentino, M., Taehyun, K., and Franco N.C. Wong. AIP Conference Proceedings **734**, 211 (2004)

[7] Kaye, P., Raymond, L., and Michele, M. An Introduction to Quantum Computing. (Oxford UP, Oxford, 2007)

[8] Kwiat, P., Steinberg, A., and Raymond, C. Physical Review A **45**, 11 (1992)

[9] Pittman, T.B., Strekalov, D.V., Migdall, A., Rubin, M.H., Sergienko, A.V., and Shih, Y.H. Physical Review Letters **77**, 10 (1996)

[10] Sergienko, A.V., Shih, Y.H., Rubin, M.H. Journal of the Optical Society B **12**, 5 (1995)

[11] Tosi, G., Mohiyaddin, FA., Tenberg, S., Rahman, R., Klimeck, G., and Morello, A. *APS March Meeting 2016. http://arxiv.org/pdf/1509.08538v1.pdf*